The coexistence of pressure waves in the operation of quartz-crystal shear-wave sensors

S. M. Reddy, J. P. Jones, and T. J. Lewis

The coexistence of pressure waves in the operation of quartz-crystal shear-wave sensors

S. M. Reddy, J. P. Jones, and T. J. Lewis[a)]
Institute of Molecular and Biomolecular Electronics, SEECS, University of Wales, Bangor,
Gwynedd LL57 1UT, United Kingdom

It is demonstrated that an AT-cut quartz crystal driven in the thickness-shear-wave mode and typically used as a sensor to monitor the viscoelastic shear-wave properties of a fluid also produce longitudinal pressure waves. Unlike the shear wave, these waves are capable of long-range propagation through the fluid and of reflection at its boundaries, notably at an outer fluid–air interface. They introduce a component into the measured electrical impedance and resonance frequency shift of the crystal, which reflects the setting up of cyclic pressure-wave resonances in the fluid. This has important implications for the practical employment of these crystal as sensors. Under appropriate conditions, as demonstrated for water and *n*-octane, it is possible to determine the propagating properties of sound waves in a fluid simultaneously with the viscoelastic shear-wave properties. These experiments are supported by an analysis of the appropriate hydrodynamic equations for waves in the crystal–fluid system, which predicts electrical characteristics in close agreement with those found experimentally. © *1998 American Institute of Physics.*
[S0021-8979(98)00205-9]

I. INTRODUCTION

AT-cut piezoelectric quartz crystals, driven in the thickness-shear mode and immersed in a fluid are being used in many applications to monitor the viscoelastic properties of the fluid at the crystal surface. It is generally assumed that the crystal generates a simple propagating shear wave which, interacting with the fluid, causes a mechanical load on the crystal. The piezoelectric coupling then allows this load to be interpreted in terms of changes in the resonance frequency and electrical impedance of the crystal.

This ideal situation is unlikely to be attained in practice, however, because of the boundary conditions at the crystal surface. In the first place, as Martin and Hager[1,2] have emphasized, since the circular electrodes are necessarily finite, the tangential surface velocity of an AT-cut crystal is nonuniform, having a Gaussian profile with a maximum at the center and falling to zero just beyond the electrode edge. They have argued[1] that this nonuniform motion in the plane of the crystal, in addition to causing the expected shear motion, will also produce a component of fluid motion normal to the crystal surface. Indeed, they and others[3,4] have demonstrated experimentally that this fluid motion does occur with a wave propagating away from the crystal surface. However, as will be shown below, the Martin and Hager analysis of the origin of this wave is unsatisfactory.

Second, there is considerable evidence that a normal as well as a tangential velocity is actually generated at the surface of these crystals. While the latter might be deliberately generated piezoelectrically, the former arise from coupled flexural motions of the crystal as Mindlin,[5] Koga,[6] and others have described. Indeed, Mindlin argues that the resonances

in a bounded crystal commonly distinguished as those of the thickness–shear modes are simply regions in the spectrum of flexural mode resonances where the frequency is least sensitive to crystal dimensions. Although their analyses were applied to rectangular quartz plates, the general findings will apply to circular plates as considered here. Thus, the piezoelectrically excited thickness–shear mode vibrations in finite planar crystals such as those commonly employed as sensors will require the coexcitation of flexural modes to satisfy the crystal conditions. Moreover, each mode will generate both normal and tangential components of velocity and displacement at the crystal surface. Although the flexural mode does not contribute significantly to the tangential displacement, its contribution to the normal displacement is some four times that of the shear mode.[5]

The consequences of this situation are explored below. First, it is shown that in experiments where AT-cut crystals are used in typical fluids having a free surface and the resonance frequencies and electrical impedances are monitored, there is clear evidence that both transverse shear (S) and longitudinal pressure (P) waves contribute to the measured properties. This confirms and extends the experimental evidence given earlier.[1–4]

Second, removing the restriction of incompressibility, and considering the full hydrodynamic equations for a viscoelastic fluid, the particle velocity in the fluid can be decomposed into component velocities transverse and normal to the crystal surface, which are compatible with the transverse shear and flexural modes excited at the crystal boundary. These components give rise, respectively, to S and P waves. This treatment is in contrast to that of Martin and Hager[1] and Lin and Ward[3] in which the assumption that the fluid was incompressible was made.

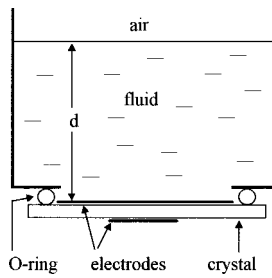[a)]Electronic mail: seecs@sees.bangor.ac.uk

FIG. 1. The fluid cell and quartz-crystal system.

It is then possible to derive expressions for the resonance frequency and electrical impedance of the crystal/fluid system, which show good correlation with those obtained experimentally for the typical fluids water and *n*-octane and from which it is possible to obtain values of the sound velocity simultaneously with the shear-wave properties. These findings have implications for the practical employment of AT-cut quartz crystals as sensors of viscoelastic loads.

II. EXPERIMENT

AT-cut planar quartz crystals, 0.16 mm thick, operating as thickness–shear resonators at a nominal fundamental resonance frequency of 10 MHz were used. The crystals had 200 nm thick gold electrodes, the upper one 7 mm and the lower one 3 mm in diameter. A crystal was mounted in the base of a 30 mm diam cylindrical metal cell, using an O-ring compression seal as shown in Fig. 1. The upper surface was in contact with a column of liquid, d, approximately 5 mm deep and the lower surface was in air. The cell was adjusted so that the crystal and liquid surfaces were approximately parallel. The depth d could be very gradually changed with time, either by allowing natural evaporation to occur or by means of a peristaltic pump. An impedance analyzer (Hewlett Packard model 4194A) was used to measure the electrical impedance of the crystal as a function of frequency. All measurements were made at a temperature of approximately 20 °C. A typical response for the crystal in contact with water of fixed depth ~5 mm is shown in Fig. 2. The modulus of the impedance is characterized by a minimum $|Z_e^\sigma|$ and a maximum $|Z_e^\pi|$, which are attributable to the series (σ) and parallel (π) shear-wave resonances of the system at frequencies f^σ and f^π, respectively.
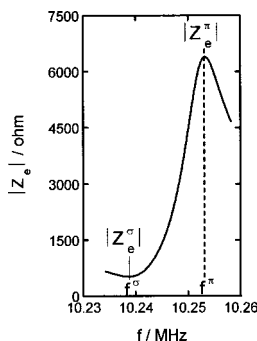

FIG. 2. The modulus $|Z_e|$ of the electrical impedance of the crystal in water near the series and parallel resonance frequencies f^σ and f^π.
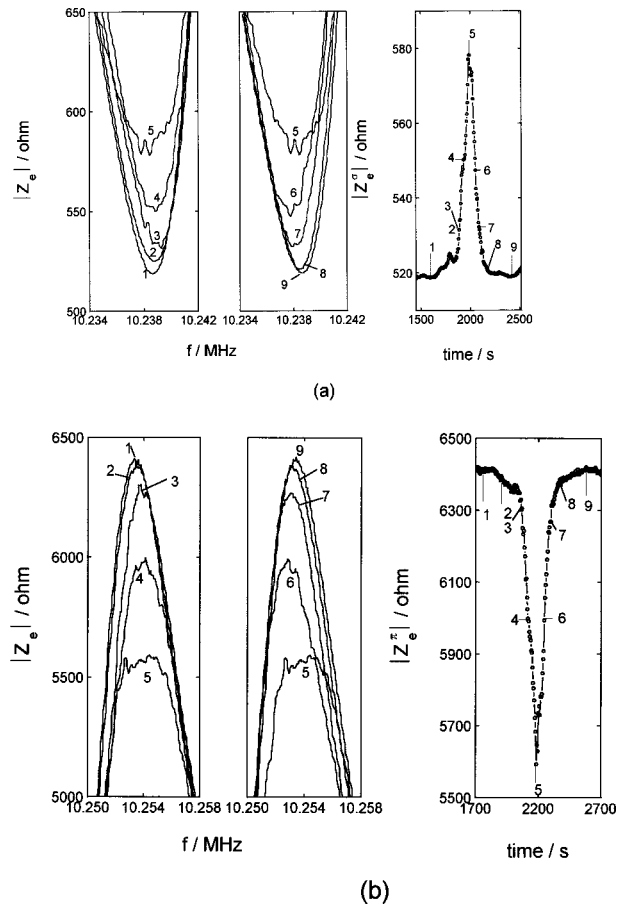

FIG. 3. Cyclic changes in $|Z_e|$ as the depth d of water in the cell is gradually decreased with time through the sequence 1–9 at frequencies near to the resonances (a) at f^σ and (b) at f^π. Also shown are the corresponding changes in the minimum $|Z_e^\sigma|$ at the series resonance and maximum $|Z_e^\pi|$ at the parallel resonance.

It was observed that the responses were sensitive to the depth, d, of the fluid, the modulus $|Z_e|$ undergoing small cyclic changes as d was gradually increased or decreased. An example for water showing this behavior in the neighborhood of the f^σ and f^π resonance frequencies is given in Fig. 3. The changes can be seen most clearly in the resonance impedances $|Z_e^\sigma|$ and $|Z_e^\pi|$, which show a regular succession of maxima and minima, respectively, as d is changed with time (Fig. 4). The associated resonance frequencies f^σ and f^π are also shown and are clearly indicative of additional secondary resonances superimposed on the main shear-wave resonances. From a knowledge of the area of the liquid/air interface, the change in water depth, Δd, required to move through one cycle of a secondary resonance could be determined. In the case of natural evaporation, this was done by measuring the loss in weight over a given time in an auxiliary experiment and, when the pump was employed, by determining the pumping speed (usually, 60 nL/s). For water, Δd was 74.1 μm.

The secondary resonances were sensitive not only to the depth of the liquid but also to the general geometry of the cell. Cells of larger diameter gave similar performance, while insertion of metal rings into the 30 mm cell to reduce the diameter of the liquid column so that the liquid/air meniscus
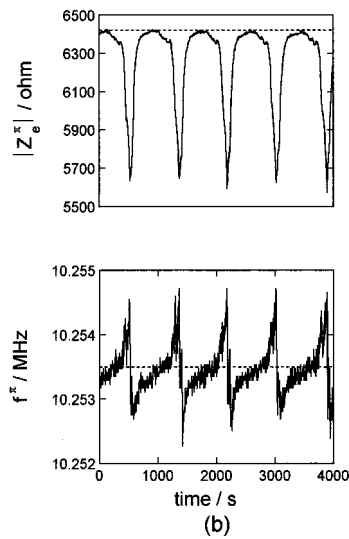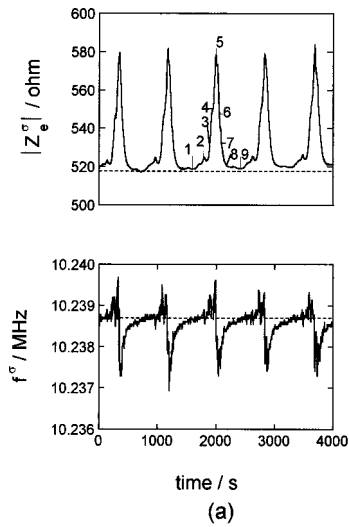
FIG. 4. Sequences of (a) maxima in $|Z_e^\sigma|$ and (b) minima in $|Z_e^\pi|$ as the water depth d is changed linearly with time. The corresponding changes in resonance frequencies f^σ and f^π are also shown. The numbered sequence in (a) corresponds to that in Fig. 3(a).

became more prominent, produced a number of additional resonances. Slightly tilting the cell from the vertical so that the liquid surface was no longer parallel to the crystal surface also introduced additional resonances as shown in Fig. 5, and a more severe tilting produced a much broader response suggesting resonances over a continuous range of depths (Fig.
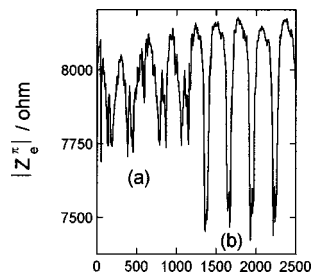

FIG. 5. Effect on $|Z_e^\pi|$ when the crystal surface and water–air interface are not parallel. A small misalignment produces double peaks (a) and improved alignment results in single peaks (b).
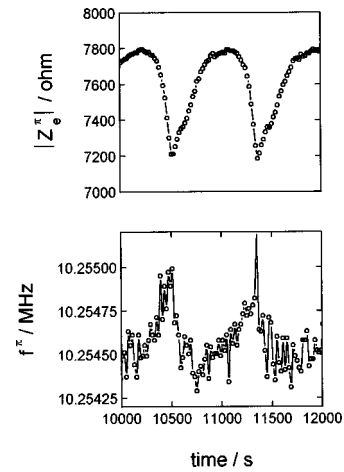

FIG. 6. Effect of severe misalignment of crystal surface and water–air interface.

6). These results were not specific to water, and similar phenomena occurred with other liquids including aqueous solutions. For example, Fig. 7 shows the resonance sequences for n-octane under natural evaporation. In this case, a small degree of nonalignment produced a small but well-separated second resonance.

Shear waves in liquids are expected to be absorbed within a few μm of the crystal surface, and therefore, the shear-wave impedance should be insensitive to the depth and configuration of the fluid volumes employed here. It appears that the depth-sensitive secondary resonances arise from waves that are capable of propagation through the liquid and reflection at the liquid/air interface, and therefore, must be longitudinal pressure or P waves. Provided the crystal surface and liquid–air interface are parallel, the cell can then be ''tuned'' to give reasonably sharp single resonances by adjusting the liquid depth as in Fig. 4. Otherwise, given the configuration of the fluid volume and the possibility of multiple paths within it, confused responses are to be expected. The situation is reminiscent of that for the liquid acoustic interferometers described by Hubbard[7] and particularly by Hunter and Fox[8,9] who used the reflecting qualities of the air–liquid interface in obtaining resonances in a column of oil driven by a quartz crystal operating in the thickness expander, P-wave, mode. These authors emphasized that con-
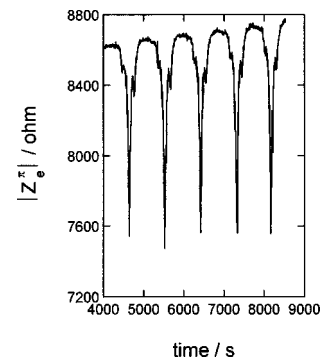

FIG. 7. Resonance sequences for n-octane as depth d is reduced by natural evaporation.

siderable care was necessary in leveling the resonator if a pure resonance was to be achieved and unwanted secondary modes avoided.

A repeat of the resonance sequence will occur as the liquid level alters whenever the depth d changes by a half wavelength of the pressure wave established in the liquid. Thus, the change in depth Δd between resonances in the sequences shown in Figs. 4 and 7 should be equal to $\lambda/2$, where $\lambda = c/f$ is the wavelength at frequency f and c is the velocity of pressure waves in the liquid. From these measurements, the wave velocities in water and n-octane are deduced to be 1517 and 1231 m s^{-1}, respectively, in remarkably good agreement with published values of the sound velocities in these liquids.[10]

The observed effects confirm the presence of a pressure (P) wave component generated by the crystal simultaneously with the normal shear (S) wave and contributing to the overall mechanical impedance of the liquid sensed by the crystal. This component is particularly sensitive to the setting up of resonance conditions within the liquid column, and extraneous fluctuations in the liquid depth will be reflected in fluctuations in the measured resonance frequency and in the resonance impedances $|Z_e^\sigma|$ and $|Z_e^\pi|$. This can be seen in Fig. 3 where vibration-induced ripples in the liquid surface are manifest as fluctuations in the $|Z|$ characteristics, particularly close to the turning points.

III. SIMULTANEOUS GENERATION OF S AND P WAVES

To explore the coexistence of transverse S and longitudinal P waves, it is necessary to consider the hydrodynamic equations for a fluid that is both viscous and compressible. By contrast, in earlier treatments[1,3] it was assumed that the fluid was incompressible and an incomplete hydrodynamic equation was employed in which a pressure term was omitted. It was argued that the nonuniform tangential surface velocity of the crystal gave rise to a velocity in the fluid normal to the crystal surface. The treatment is ultimately unsatisfactory, however, because this velocity does not have the attributes of a traveling wave as observed experimentally, although the authors suggested that one might be generated beyond the viscous boundary layer at the crystal surface. In fact, the assumption of incompressibility implies that a longitudinal P wave cannot propagate and so their treatment must inevitably fail to predict one.

In the Appendix, the linearized hydrodynamic equations of motion[11] are considered for a compressible, viscoelastic fluid and it is found convenient to decompose the particle velocity $\bar{v}$ into two components $\bar{v}_1$ and $\bar{v}_2$ where

$$\bar{v}_1 = \text{curl } \psi, \quad \text{and} \quad \bar{v}_2 = \text{grad } \phi,$$

in which ψ and ϕ are vector and scalar velocity potentials. A coordinate system is adopted in which axes x and y are in the plane of the crystal surface and z is normal to it. At the crystal surface, the piezoelectric drive is assumed to induce a primary motion in the x direction but a component in the z direction is also assumed because of the possibility of flexural modes.[5] The treatment by Schneider and Martin[4] includes the compressibility of the liquid but does not consider

flexural motion, arguing instead that a pressure wave is generated solely by the variation of lateral motion across the crystal surface.

The velocity $\bar{v}_1$ satisfies Eq. (A6) and depends on the fluid viscoelasticity η, which under an alternating shear stress, can be expressed as $\eta^* = \eta' - i\eta''$ where η' and η'' are energy loss and storage components. $\bar{v}_1$ has a major component in the x direction [Eq. (A13)], which can be expressed as

$$v_{1x} = V_x e^{i(\omega t - k_1 z)} f(x,y),$$

where $V_x f(x,y)$ is the magnitude of the tangential thickness–shear mode velocity generated by the crystal at the surface $z = 0$ and $f(x,y)$ accounts for the variation of this velocity across the crystal face. $f(x,y)$ is found to be of Gaussian form.[2–4] The velocity v_{1x} is that of a transverse shear, S wave, propagating in the z direction with an angular frequency ω. (In the physical interpretation of v_{1x} the real component of $e^{i\omega t}$ is to be taken). The wave-number k_1 is complex and can be written as

$$k_1 = \pm (\omega \rho_0 / |\eta|)^{1/2} e^{-i\theta/2}, \tag{A12}$$

where $|\eta| = (\eta'^2 + \eta''^2)^{1/2}$ and $\theta = \tan^{-1} \eta'/\eta''$. Thus, v_{1x} is entirely associated with the viscoelastic shear-wave properties of the fluid and has the characteristics of the expected shear wave generated by the crystal. Absorption occurs because k_1 has an imaginary component. There is also a z-directed wave v_{1z} generated wherever $\partial f(x,y)/\partial x$ is nonzero [Eq. (A14)], but this is likely to be much less than v_{1x}. It is similar to the normally directed wave component described by Martin and Hager[1] and is attenuated to the same degree as the S-wave v_{1z}. Consequently, it can be overwhelmed by a true propagating longitudinal wave in the z direction associated with v_2 as described below.

The v_{1x} S wave will generate a shear stress at the crystal surface of magnitude $\eta^*(\partial v_{1x}/\partial z)_0$ and will give rise to a shear impedance

$$\bar{Z}_s = S_s \eta^* \left(\frac{\partial v_{1x}}{\partial z}\right)_0 [v_{1x}(0)]^{-1},$$

where S_s is the active area of the crystal for S waves. From Eq. (A13)

$$\bar{Z}_s = -i S_s \eta^* k_1,$$

and using Eqs. (A11) and (A12),

$$\bar{Z}_s = S_s (\omega \rho_0 \eta)^{1/2} e^{i\theta/2},$$

which can be expressed as

$$\bar{Z}_s = R_s + iX_s.$$

On the other hand, the velocity component $\bar{v}_2$, satisfies Eq. (A7), which includes a term involving the pressure p and thereby admits the possibility of longitudinal pressure waves in the fluid. It also involves a term containing the viscoelastic coefficients η and ζ, (the second coefficient ζ relating to the fluid compressibility[11]). The solution of Eq. (A7) yields a dominant longitudinal P-wave v_{2z} [Eqs. (A16) and (A18)],
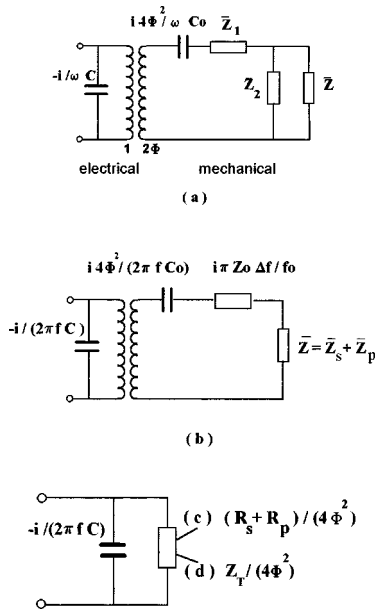
FIG. 8. (a) and (b) equivalent electrical–mechanical circuits for the crystal system. (c) Circuit for series mechanical resonance. (d) Circuit for parallel electrical resonance.

which propagates through the fluid with a phase velocity c and absorption coefficient α [Eq. (A17)], which depend on η^* and ζ^*.

This wave will undergo multiple reflections at the fluid–air and fluid–crystal interfaces creating a load impedance $\overline{Z}_p$ on the crystal given by Eq. (A19), which can be expressed as

$$\overline{Z}_p = R_p + iX_p,$$

where

$$R_p = S_p\rho c\, \frac{(1-r^2\gamma^2)[1+\tan^2(\omega d/c)]}{(1-r\gamma)^2+(1+r\gamma)^2\,\tan^2(\omega d/c)}, \quad (1)$$

$$X_p = -S_p\rho c\, \frac{4r\gamma\,\tan(\omega d/c)}{(1-r\gamma)^2+(1+r\gamma)^2\,\tan^2(\omega d/c)}, \quad (2)$$

and γ is the absorption factor $e^{-2\alpha d}$. The velocity reflection coefficient r, in an ideal case would be $+1$, but in the present case the reflector is a free fluid–air interface locally perturbed by the P wave as well as by extraneous vibrations and r is likely to be <1.

IV. THE ELECTRICAL IMPEDANCE

It is now necessary to interpret the combined mechanical impedance $(\overline{Z}_s+\overline{Z}_p)$ in terms of the electrical impedance of the crystal. Following Thurston[12] and Johannsmann et al.,[13] the equivalent electrical–mechanical circuit is as shown in Fig. 8(a) where

$$\overline{Z}_1 = -2iZ_0\cot\frac{\omega h}{v_q}, \quad \overline{Z}_2 = 2iZ_0\tan\frac{\omega h}{v_q},$$

and

$$\overline{Z} = \overline{Z}_s + \overline{Z}_p = R + iX = (R_s + R_p) + i(X_s + X_p).$$

The crystal impedance $Z_0 = S_s\rho_q v_q$, where ρ_q is the density and v_q the shear-wave velocity for quartz, h is the half thickness of the crystal, Φ^2 is the piezoelectric ratio of mechanical to electrical impedance,[12] C_0 is the electrical capacitance of the crystal, and C is the total capacitance (C_0 plus stray capacitance) at the input terminals of the crystal.

At a frequency f in the neighborhood of the fundamental crystal resonance $f_0(=v_q/4h)$, i.e., where $f=f_0+\Delta f$,

$$\overline{Z}_1 \approx i\,\pi Z_0\Delta f/f_0,$$

and $\overline{Z}_2$ is large and can be neglected in comparison with the parallel load impedance $\overline{Z}$. Accordingly, the equivalent circuit is then as in Fig. 8(b).

The condition for a series *mechanical* resonance at a frequency f^σ near to f_0 is that the total reactive component of the mechanical impedance is zero, i.e., that

$$\frac{2\Phi^2}{\pi f^\sigma C_0} + \frac{\pi Z_0(f^\sigma - f_0)}{f_0} + X = 0. \quad (3)$$

In the first term, f^σ may be replaced by f_0 with insignificant error. If Δf^σ is defined as the difference between the mechanical series resonance frequencies of the crystal immersed in a fluid, f^σ, and in air, f'_0, then to a good approximation since $X\approx 0$ in the latter case,

$$\Delta f^\sigma = \Delta f^\sigma_s + \Delta f^\sigma_p = -\frac{f_0(X_s + X_p)}{\pi Z_0}, \quad (4)$$

where Δf^σ_s and Δf^σ_p are the separate contributions from the S- and P-wave reactances. There is an implied assumption here that the piezoelectric ratio Φ is the same for the shear and flexural modes. This point will be discussed later.

At series mechanical resonance only the real element, $(R_s + R_p)$ of the mechanical impedance remains and the electrical impedance is obtained by transferring this through the transformer to the electrical side [Fig. 8(c)]. The modulus of the electrical impedance then becomes

$$|\overline{Z}^\sigma_e| = \frac{R_s+R_p}{4\Phi^2}\left\{1+\left[\frac{\pi f_0 C(R_s+R_p)}{2\Phi^2}\right]^2\right\}^{-1/2} \quad (5)$$

where f^σ has been replaced by f_0.

The mechanical impedance transferred to the electrical side is shunted by the input capacitance C, and consequently, a parallel electrical resonance is also possible at a frequency $f^\pi > f^\sigma$. Assuming that f^π is close to f_0 so that Fig. 8(b) applies, the total mechanical impedance $\overline{Z}_T = (R_s + R_p) + iX_T$ of the components represented in Fig. 8(b) may be transferred to the electrical side, giving an equivalent electrical impedance $Z_T/4\Phi^2$ [Fig. 8(d)]. The total electrical impedance is then

$$\overline{Z}^\pi_e = \frac{\overline{Z}_T}{4\Phi^2 + i2\pi f^\pi C\overline{Z}_T}. \quad (6)$$

The condition for parallel resonance is that the reactive part of $(\overline{Z}^\pi_e)^{-1}$ is minimized, which requires that

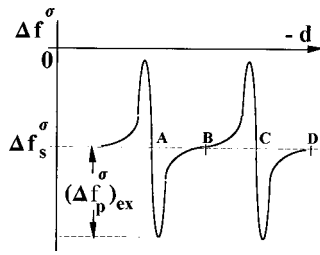$$X_T = \frac{2\Phi^2}{\pi f^\pi C}. \quad (7)$$

FIG. 9. The shift in the series resonance Δf^σ as the depth d of the fluid is decreased. Zeros in Δf_p^σ occur where $d=n\lambda/4$ (at A, C, etc., when n is even and B, D, etc., when n is odd).

The expression for X_T at resonance f^π is the left-hand side of Eq. (3) with f^σ replaced by f^π, and thus,

$$\Delta f^\pi = \frac{-f_0(X_s+X_p)}{\pi Z_0} + \frac{2\Phi^2}{\pi^2 Z_0 C}. \qquad (8)$$

Using Eqs. (6) and (7), the modulus of the impedance at parallel resonance becomes

$$|Z_e^\pi| = \frac{\Phi^2}{(\pi f^\pi C)^2 (R_s+R_p)}\left[1+\left(\frac{\pi f^\pi C(R_s+R_p)}{2\Phi^2}\right)^2\right]^{1/2}. \qquad (9)$$

The way in which the measured parameters Δf^σ, Δf^π, $|Z_e^\sigma|$, and $|Z_e^\pi|$ might change as the fluid depth d is altered can now be determined. Unless d is within the absorption range of the shear wave ($\sim 10\ \mu\mathrm{m}$), an unlikely condition in normal operation of the crystal as a sensor in a fluid, R_s and X_s will be independent of d. On the other hand, R_p and X_p, [Eqs. (1) and (2)] are cyclic functions of d.

If it is assumed that the variation of γ with d is of second order compared with the variation of $\tan(\omega d/c)$, then, from Eq. (2), X_p will have zeros where $\omega d/c=n\pi/2$, n being an integer, i.e., where $d=n\lambda/4$, λ being the wavelength. X_p also has turning points where, for n even,

$$d = \frac{n\lambda}{4} \pm \frac{\lambda}{2\pi}\tan^{-1}\frac{1-r\lambda}{1+r\lambda}.$$

At these points, the reactance has extreme values

$$\mu\,\frac{2r\gamma Z_f}{1-r^2\gamma^2},$$

in which $Z_f=S_p\rho c$, the characteristic P-wave impedance of the fluid. Using Eq. (8), the corresponding extreme shifts in Δf_p^σ are

$$(\Delta f_p^\sigma)_{\mathrm{ex}} = \pm\frac{2r\gamma f_0 Z_f}{(1-r^2\gamma^2)\pi Z_0}. \qquad (10)$$

Thus, as shown in Fig. 9, when d is progressively changed, the presence of the P wave causes Δf^σ [Eq. (4)] to oscillate about a mean value, Δf_s^σ, (the shift in series resonance frequency induced by the S-wave load) by an amount Δf_p^σ. According to Eq. (8), Δf^π, the shift in the parallel resonance frequency, will show similar oscillatory behavior.

Comparison of Figs. 9 and 4 shows how well the model predicts the character of the experimental results and confirms the earlier supposition that a P wave was present. [Note that in Fig. 9 the abscissa corresponds to decreasing
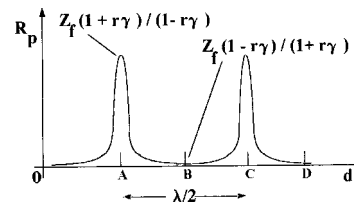

FIG. 10. R_p as a function of d. When $d=n\lambda/4$, maxima occur for n even (A, C, etc.,) and minima for n odd (B, D, etc.,).

depth d as in Fig. 4.] Small fluctuations on the traces in Fig. 4 are likely to be due to perturbations in the liquid–air interface already discussed.

R_p, the real part of $\bar{Z}_p$ [Eq. (1)] is also a cyclic function of d. When $d=n\lambda/4$, maxima equal to

$$Z_f(1+r\gamma)/(1-r\gamma),$$

occur for n even and minima equal to

$$Z_f(1-r\gamma)/(1+r\gamma),$$

for n odd as shown in Fig. 10. The width of a peak in R, defined by the interval in d over which Δf_p^σ goes from $-(\Delta f_p^\sigma)_{\mathrm{ex}}$ to $+(\Delta f_p^\sigma)_{\mathrm{ex}}$ [Eq. (10)], is

$$\frac{\lambda}{2}\left[\pi - 2\tan^{-1}(1-r\gamma)/(1+r\gamma)\right].$$

The periodicity in R_p will be reflected in the resonance impedances $|Z_e^\sigma|$ and $|Z_e^\pi|$ [Eqs. (5) and (9)] and, in both cases, the effect of R_p under the square-root sign will be of second order. Accordingly, to a first approximation, $|Z_e^\sigma|$ may be expected to vary directly with R_p and as d is gradually changed, to go through a series of maxima of magnitude

$$|Z_e^\sigma|_{\max} \approx \left[\frac{Z_f(1-\gamma)}{1+\gamma}+R_s\right](4\Phi^2)^{-1},$$

as shown in Fig. 11.

In the case of $|Z_e^\pi|$ the situation is somewhat more complicated, but if $R_p \ll R_s$, a condition applicable to water and to n-octane, then

$$|Z_e^\pi| \approx \frac{\Phi^2}{(\pi f_0 C)^2 R_s}\left(1-\frac{R_p}{R_s}\right),$$

which varies linearly with R_p, and thus, will also be cyclic in d (Fig. 11). Note that $|Z_e^\pi|$ is maximum where $|Z_e^\sigma|$ is
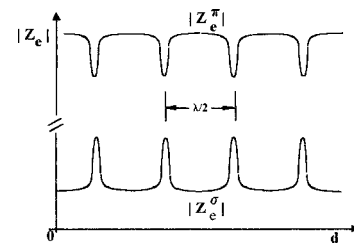

FIG. 11. The cyclic nature of the series and parallel resonance impedances $|Z_e^\sigma|$ and $|Z_e^\pi|$, as d is increased.

minimum. These characteristics of the model are closely similar to those of the experimental results shown in Figs. 4 and 7.

There are two main reasons why it is not possible to predict accurately the relative magnitudes of the transverse and longitudinal wave impedances. First, the electromechanical conversion ratio, Φ^2, is not necessarily the same for the thickness–shear and flexural modes. Second, the active areas S_s and S_p involved in the impedances cannot be assumed to be the same although S_s is likely to be approximately equal to the nominal area of the crystal electrode. However, assuming Φ to be the same for the two modes, it is possible to obtain an estimate of S_p/S_s as follows.

Since $Z_p = S_p z_w$ and $Z_0 = S_s z_q$, where z_w, z_q are the characteristic impedances for the P wave in the fluid (water) and for an S wave in quartz (1.5×10^6 and 8.8×10^6 kg m^{-2} s^{-1}, respectively), Eq. (10) can be converted to

$$\frac{S_p}{S_s} = 9.1 \frac{(1 - r^2 \gamma^2)}{r \gamma} \frac{(\Delta f_p^\sigma)_{\text{ex}}}{f_0}.$$

In the case of water,[10] the absorption coefficient at 10^7 Hz is 2.5 Np m^{-1}, and thus, for a depth $d = 5$ mm, $\gamma = 0.975$ while, from Fig. 4, $(\Delta f_p^\sigma)_{\text{ex}}/f_0$ is about 10^{-4}. Thus, if the interface is ideal, $r = 1$ and $S_p/S_s \approx 5 \times 10^{-5}$, while if it is rough and r is small, say 0.1, then $S_p/S_s \approx 10^{-2}$. In either case, only a small area of the crystal surface appears to support the P wave. This is not surprising if the tuning requirement for a P wave is considered. Resonance will be achieved only where d is a multiple of $\lambda/2$. In addition to any lack of parallelism between the crystal and fluid/air interfaces, the topology of the crystal surface and the existence of ripples in the fluid surface will lead to a variation in depth across the crystal face and a distribution of d values. In this situation, resonance conditions will exist only locally. In the case of water, for example, the wavelength of the P wave will be about 150 μm and tuning to resonance will require adjustment in depth to within a μm or so. Variations in d of this order across the crystal face are very likely to occur and will mean that only localized resonances will be possible at any one time. In these circumstances, the effective S_p can be expected to be much less than S_s.

V. CONCLUSIONS

It has been shown that a typical AT-cut crystal sensor system, operating in a nominally thickness–shear mode in a liquid, can generate a longitudinal P wave as well as the expected transverse S wave, the former being sufficiently strong to affect the overall sensor performance. The accompanying analysis assumes that the mechanical impedances associated with the two waves are to be considered in series and transformed with the same transformer ratio Φ to the electrical side. The general agreement between theory and experiment indicates that this is a plausible procedure. If Φ were different for the thickness–shear and flexural modes, the weight given to each impedance on the electrical side

would be altered without affecting the general conclusions, although the estimate of the effective area associated with the P wave would be altered.

Unlike S waves, the weak absorption of P waves means that they can have long-range interactions with the crystal surroundings. The frequency shift Δf and impedance $\bar{Z}_e$ reflect these interactions. In a given configuration of operation of a crystal sensor in a fluid, the P-wave contribution to the overall frequency shift and impedance determined by the crystal might be unsuspectingly attributed to shear waves. The P-wave paths will involve reflections at any of the boundaries of the sensor/fluid cell, but those involving the liquid–air boundary (or a liquid–metal boundary in cases where the crystal is mounted vertically in the wall of a cell) will be particularly important because the reflection coefficient could approach unity there. Unless they are well controlled, the P-wave contributions will at least introduce ''noise'' and drift into the sensor response.

On the other hand, once the existence of P waves is recognized, they may be used to make meaningful measurements of the pressure-wave velocity in the bulk fluid simultaneously with the S-wave viscoelastic studies at the crystal–fluid boundary. By careful cell design, it might be possible to use the P wave for a more extensive study of the pressure-wave properties of a fluid simultaneously with the shear-wave properties, so obtaining information on all the viscoelastic parameters of the fluid.

ACKNOWLEDGMENTS

APPENDIX

The linearized hydrodynamic equations of motion for a viscoelastic compressible fluid[11] are

$$\rho \frac{d\bar{v}}{dt} = -\text{grad } p + \eta \Delta \bar{v} + (\zeta + \eta/3) \mathbf{\nabla} \cdot \mathbf{\nabla} \bar{v}, \quad \text{(A1)}$$

and

$$\frac{d\rho}{dt} + \text{div}(\rho \bar{v}) = 0, \quad \text{(A2)}$$

where $\bar{v}$ is the particle velocity, ρ is the excess density $\ll \rho_0$, the equilibrium value, and p is the excess pressure $\ll p_0$, the corresponding equilibrium pressure. ζ and η are viscoelastic coefficients, the former appearing when the fluid is compressible.

It is convenient to decompose the particle velocity into two components[14] so that

$$\bar{v} = \bar{v}_1 + \bar{v}_2,$$

where

$$\bar{v}_1 = \text{curl } \psi, \quad \bar{v}_2 = \text{grad } \phi. \quad \text{(A3)}$$

Then

$$\text{div } \bar{v}_1 = 0,$$

and, since curl grad $\phi = 0$,

$$\nabla \cdot \nabla \bar{v} = \nabla \cdot \nabla \bar{v}_2 = \Delta \bar{v}_2.$$

Equations (A1) and (A2) may then be written as

$$\left(\rho_0 \frac{\partial \bar{v}_1}{\partial t} - \eta \Delta \bar{v}_1 \right) + \left(\rho_0 \frac{\partial \bar{v}_2}{\partial t} - \left[\zeta + \frac{4\eta}{3} \right] \Delta \bar{v}_2 + \text{grad } p \right) x = 0, \tag{A4}$$

$$\frac{\partial \rho}{\partial t} + \rho_0 \text{ div } \bar{v}_2 = 0. \tag{A5}$$

Clearly, the decomposed representation of $\bar{v}$ satisfies Eq. (A4) if

$$\rho_0 \frac{\partial \bar{v}_1}{\partial t} - \eta \Delta \bar{v}_1 = 0, \tag{A6}$$

and

$$\rho_0 \frac{\partial \bar{v}_2}{\partial t} - \left(\zeta + \frac{4\eta}{3} \right) \Delta \bar{v}_2 + \text{grad } p = 0. \tag{A7}$$

Adopting a Cartesian coordinate system in which axes x, y are in the plane of the crystal surface and z is normal to the surface and assuming that the piezoelectric drive induces a surface motion primarily in the x direction so that $v_{1y} \sim 0$, then, according to Eq. (A3), ψ will have only a y component, ψ_y, and

$$v_{1x} = -\frac{\partial \psi_y}{\partial z}, \quad v_{1y} = 0, \quad v_{1z} = \frac{\partial \psi_y}{\partial x}. \tag{A8}$$

Thus, Eq. (A6) becomes

$$\rho_0 \frac{\partial \psi_y}{\partial t} = \eta \Delta \psi_y, \tag{A9}$$

an equation of heat conduction type. A simple plane-wave solution propagating in the z direction is

$$\psi_y = A e^{i(\omega t - k_1 z)} f(x,y), \tag{A10}$$

where A can be complex and is determined by boundary conditions at the crystal surface and $f(x,y)$ accounts for the variation of the surface velocity $v_{1x}(z=0)$ across the crystal face. ω and k_1 are the frequency and wave number, respectively. Substituting into Eq. (A9), the wave number is found to be complex and is given by

$$k_1^2 = -\frac{i\omega\rho_0}{\eta^*}, \tag{A11}$$

where $\eta^* = \eta' - i\eta''$ in which η' and η'' are the viscous and elastic components of the viscoelasticity coefficient at the frequency ω. Hence,

$$k_1 = \pm \left(\frac{\omega\rho_0}{|\eta|} \right)^{1/2} e^{-i\theta/2}, \tag{A12}$$

where $|\eta| = (\eta'^2 + \eta''^2)^{1/2}$ and $\theta = \tan^{-1} \eta'/\eta''$. For a Newtonian liquid, $\eta'' = 0$, $\eta = \eta' = \eta_s$, and $\theta = \pi/2$, so that $k_1 = \pm(1-i)(\omega\rho_0/2\eta_s)^{1/2}$.

Returning to Eq. (A10), using Eq. (A8), and choosing the positive root of k_1 so that ψ_y is finite everywhere,

$$v_{1x} = B e^{i(\omega t - k_1 z)} f(x,y), \tag{A13}$$

$$v_{1z} = (ik_1)^{-1} B e^{i(\omega t - k_1 z)} \partial f(x,y)/\partial x, \tag{A14}$$

where, since v_{1x} is to be real at the crystal surface ($z=0$), $B(=ik_1 A)$ is real, and A is complex.

v_{1x} is a transverse shear wave (S wave) generated as a result of an x-directed particle velocity at the crystal surface and propagating with attenuation, since k_1 is complex, into the liquid. For most liquids, the attenuation will be large. Simultaneously, a normally directed wave, v_{1z}, phase shifted by a factor $(ik_1)^{-1}$ with respect to v_{1x}, is generated wherever $\partial f(x,y)/\partial x$ is nonzero and this wave also propagates with attenuation into the liquid. Because of the factor k_1^{-1} [Eq. (A14)], it is expected to be much smaller in magnitude than v_{1x}.

Consider now the component $\bar{v}_2$. Equation (A7) includes a term in the pressure p, and consequently, admits the possibility of a longitudinal compression wave propagating into the fluid. The term involving viscoelastic coefficients ζ and η represents energy dissipation[11] and will be responsible for absorption of the wave. If this term is temporarily neglected, Eq. (A7) becomes

$$\rho_0 \frac{\partial \bar{v}_2}{\partial t} + \text{grad } p = 0,$$

and, substituting for v_2 from Eq. (A3),

$$p = -\rho_0 \frac{\partial \phi}{\partial t}. \tag{A15}$$

The induced pressure change p will be related to the density change ρ via a modulus of compressibility $(\partial\rho/\partial p)/\rho_0$, and using this expression together with Eqs. (A3), (A5), and (A15) we find

$$\frac{\partial^2 \phi}{\partial t^2} = \frac{\partial p}{\partial \rho} \Delta \phi,$$

which is an equation for a wave with a phase velocity $c_0 = \sqrt{\partial p/\partial \rho}$.[11] A solution in the form of a plane wave propagating in the z direction is

$$\phi = C e^{i(\omega t - k_2 z)} g(x,y),$$

where C is determined by boundary conditions at the crystal surface and the wave number

$$k_2 = \frac{\omega}{c_0}.$$

The function $g(x,y)$ accounts for variation across the crystal face. ϕ is the velocity potential of a longitudinal compressional wave propagating into the fluid.

Using Eq. (A3), the normal and tangential particle velocities are then

$$v_{2z} = D e^{i(\omega t - k_2 z)} g(x,y), \tag{A16}$$

where $D = ik_2 C$ and

$$v_{2x} = C e^{i(\omega t - k_2 z)} \partial g(x,y)/\partial x.$$

v_{2z} is the velocity of a longitudinal (sound) wave or P wave and v_{2x} is that of a transverse wave which, because of the factor k_2, will be negligible compared with v_{2z} unless $\partial g(x,y)/\partial x$ is large.

Reintroduction of the viscoelastic term in Eq. (A7) causes the wave number to become complex and it can be expressed in the form

$$k_2 = \frac{\omega}{c} - i\alpha, \tag{A17}$$

where c is a phase velocity dependent on ζ' and η' and α an absorption coefficient, dependent on ζ'' and η'', the components of ζ^* (the complex form of ζ) and η^*.[15] The P-wave velocity now becomes

$$v_{2z} = De^{i\omega t}e^{-(\alpha + i\omega/c)z}g(x,y). \tag{A18}$$

The wave v_{2z} will propagate through the fluid to the air interface at d where it will be reflected with a reflection coefficient r (for an ideally smooth and parallel boundary $r = 1$). It will then return to be reflected at the quartz–liquid boundary and so on through a series of multiple reflections. Following Hubbard,[7] the series of reflections can be summed to give the particle velocity in the steady state as

$$v_{2z}^s = v_{2z}(+) + v_{2z}(-),$$

where the total forward and backward particle velocities are

$$v_{2z}(+) = De^{i\omega t}\frac{e^{-(\alpha + i\omega/c)z}}{1 - re^{-(\alpha + i\omega/c)2d}}g(x,y),$$

$$v_{2z}(-) = -De^{i\omega t}\frac{re^{-(\alpha + i\omega/c)(2d - z)}}{1 - re^{-(\alpha + i\omega/c)2d}}g(x,y).$$

The local pressure p is $\rho c[v_{2z}(+) - v_{2z}(-)]$, and if S_p is the active area for P waves, the impedance $\bar{Z}_p$ offered by the fluid load at the crystal surface is $(S_p p/v_{2z}^s)_{z=0}$, which becomes

$$\bar{Z}_p = S_p \rho c \frac{1 + re^{-2\alpha d}e^{-i2\omega d/c}}{1 - re^{-2\alpha d}e^{-i2\omega d/c}}. \tag{A19}$$

[1] B. A. Martin and H. E. Hager, J. Appl. Phys. **65**, 2627 (1989).
[2] B. A. Martin and H. E. Hager, J. Appl. Phys. **65**, 2630 (1989).
[3] Z. Lin and M. D. Ward, Anal. Chem. **67**, 685 (1995).
[4] T. W. Schneider and S. J. Martin, Anal. Chem. **67**, 3325 (1995).
[5] R. D. Mindlin, J. Appl. Phys. **22**, 316 (1951).
[6] I. Koga, J. Appl. Phys. **34**, 2357 (1963).
[7] J. C. Hubbard, Phys. Rev. **38**, 1011 (1931).
[8] J. L. Hunter and F. E. Fox, J. Acoust. Soc. Am. **22**, 238 (1950).
[9] J. L. Hunter, J. Acoust. Soc. Am. **22**, 243 (1950).
[10] G. W. C. Kaye and T. H. Laby, *Tables of Physical and Chemical Constants* (Longman, London, 1973).
[11] L. D. Landau and E. M. Lifshitz, *Fluid Mechanics* (Pergamon, Oxford, 1959).
[12] R. N. Thurston, in *Waves in Solids*, in *Handbook of Physics, Vol. 6, Mechanics of Solids IV*, edited by C. Truesdell (Springer, Berlin, 1974), pp. 109–308.
[13] D. Johannsmann, K. Matthauer, G. Wegner, and W. Knoll, Phys. Rev. B **46**, 7808 (1992).
[14] J. D. Achenbach, *Wave Propagation in Elastic Solids* (North Holland, Amsterdam, 1975).
[15] A. J. Matheson, *Molecular Acoustics* (Wiley-Interscience, London, 1971).